

## Upgrading flexural performance of prefabricated sandwich panels under vertical loading

M. Z. Kabir<sup>†</sup>, O. Rezaifar<sup>‡</sup> and M. R. Rahbar<sup>‡†</sup>

Department of Civil and Environmental Engineering, Amirkabir University, Tehran, Iran  
Prefabricated SAP Company, Tehran, Iran

(Received July 4, 2005, Accepted March 8, 2007)

**Abstract.** 3-D wall panels are used in construction of exterior and interior bearing and non-load bearing walls and floors of building of all types of construction. Fast construction, thermal insulation, reduced labor expense and weight saving are the most well pronounced advantage of such precast system. When the structural performance is concerned, the main disadvantage of 3D panel, when used as floor slab, is their brittleness in flexure. The current study focuses on upgrading ductility and load carrying capacity of 3D slabs in two different ways; using additional tension reinforcement, and inserting a longitudinal concentrated beam. The research is carried on both experimentally and numerically. The structural performance in terms of load carrying capacity and flexural ductility are discussed in details. The obtained results could give better understanding and design consideration of such prefabricated system.

**Keywords:** 3D panel; flexural performance; experiments; finite element.

---

### 1. Introduction

3-D wall panels are used in construction of exterior and interior bearing and non-load bearing walls and floors of building of all types of construction. This system consists of a welded wire space frame integrated with a polystyrene insulation core. The wall panel is placed in position and wythes of concrete are applied to both sides. Wall panel receives its strength and rigidity by the diagonal cross wires welded to the welded-wire fabric on each side. This combination produces a truss behavior, which provides rigidity and shear terms for full composite behavior. Fig. 1 shows schematically the 3D panel.

Salmon *et al.* (1997) presents the results of full-scale test of prototype sandwich panel under transverse loading in a vertical position. Nijhawan (1998) measured experimentally the interface shear force and designed the shear connectors. Einea *et al.* (1994) used the plastic composite diagonal elements to implement in sandwich panel as shear connector for increasing the thermal insulation of this system. The current work studies experimentally the mechanical behavior of 3D sandwich panel in order to observe the transferring load through of sandwich elements, the fracture mechanism of concrete wythes and the adequacy of steel bars designed based on ACI 318-95 and

---

<sup>†</sup> Associate Professor, Corresponding author, E-mail: [mzkabir@aut.ac.ir](mailto:mzkabir@aut.ac.ir)

<sup>‡</sup> Ph.D. Candidate

<sup>‡†</sup> Mse, Consultant Engineer

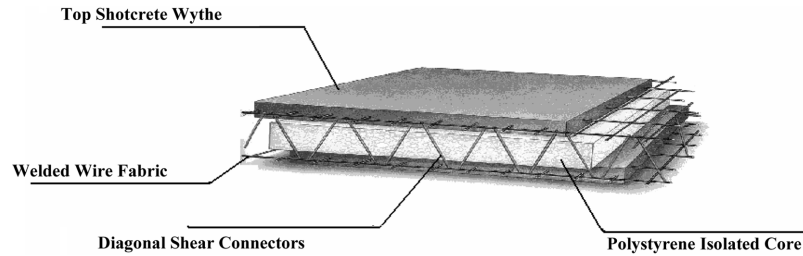


Fig. 1 3D sandwich panel

procedure of PCI design handbook 1995. PCI published comprehensive report on sandwich panels representing technical information. In 1995, Salmon *et al.* suggested mathematical solution of semi composite panels by developing differential equations and compared the analytical solution with numerical finite element analysis and showed the accuracy of their analytical method. Bush and Wu (1998), presented mathematical solution and finite element model for bending analysis of pre-stressed sandwich panels with truss diagonal shear members. Nighawan (1998), measured internal shear forces experimentally and designed shear connectors. In above literature, a technical definition of the percent of composite action is not well established. Kabir and Hasheminasab (2001), tested flexural and shear loading on 3D bearing wall and floor slab and showed the load-deflection curves and failure mechanism. Benayoune *et al.* (2005) in an experimental investigation studied the ultimate strength behaviour of precast concrete sandwich panels (PCSP), under eccentric axial loading. Deflection characteristics, variations of strains across the insulation layer, strain in shear connectors, crack appearance and propagation under increasing load were recorded and analyzed in their work Also a comprehensive experimental research in order to better understanding of mechanical characteristics of such hybrid system are conducted by the first author, 2005. The compressive strength of sprayed concrete in the form of small cores is measured as a factor of standard cylindrical specimens, Kabir and Rahbar (2005).

**2. Theoretical studies**

Computing deflections for partial-composite sandwich panels requires accounting for both the bending deformation of the concrete wythes and the relative shearing deflection between the wythes through the connecting layers. The following derivation follows that given by Holmberg and Plem (1986).

Fig. 3 shows the deformation of a differential panel element. The panel deformation consists of two components; panel curvature,  $zd\theta$ , and shearing deformation between the wythes,  $q_{,x}dx/2$ . For small displacements, the panel curvature is assumed as  $d\theta = y_{,xx}dx$ . Summing the moment due to each deformation component and rearranging yields the following

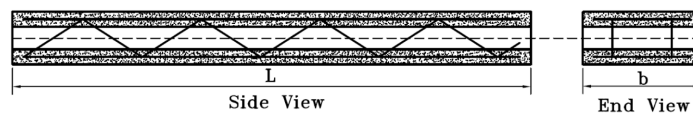


Fig. 2 Insulated sandwich panel

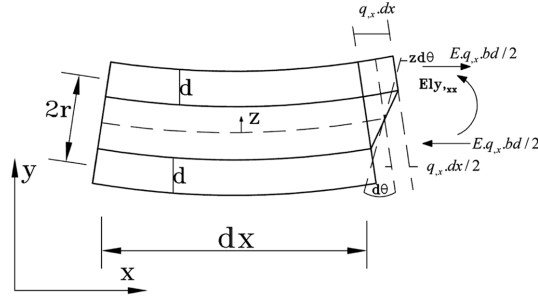


Fig. 3 Differential panel element

$$y_{,xx} = \frac{M}{EI} + \frac{\alpha^2}{2r} q_{,x} \tag{1}$$

Where  $\alpha^2 = (I - 2I_w)/I$

- $x$  : distance along the length of the panel
- $y$  : upward displacement of panel
- $q$  : relative shearing displacement between the centroid of the top and bottom wythes
- $B$  : width of the panel
- $M$  : applied moment
- $E$  : Wythe modulus of elasticity
- $I_w$  : moment of inertia of each Wythe
- $r$  : distance between structural Wythe centroids
- $d$  : structural Wythe thickness
- and  $I$  : moment of inertia of the entire panel cross section

The shear stress in the connecting layer is taken as  $Kq$  in which  $K$  is shear stiffness of connecting layer. Equilibrium of the shear forces in the connecting layer requires

$$Edy_{,xxx} - \frac{1}{2}Edq_{,xx} + Kq = 0 \tag{2}$$

Substituting the derivation of Eq. (1) into Eq. (2) and multiplying both sides by  $2/Ed$  yields the following

$$\beta^2 q_{,xx} - \chi^2 q = 2r \frac{M_{,x}}{EI} \tag{3}$$

Where  $\beta^2 = (1 - \alpha^2)$  and  $\chi^2 = 2K/Ed$ . Given the moment on the section of slabs, Eq. (3) can be solved for  $q$ . For given  $q$ , Eq. (1) can be integrated twice to give the deflection.

Boundary conditions on  $q$  and  $y$  at the panel ends,  $x = x_0$ , and  $x = x_L$  are given for three cases.

Case 1: Simply supported

Each wythe is free to rotate at both ends and the bending moment becomes zero. In addition, the overall panel moment is zero. Therefore, the following conditions are set to zero

$$y_{,xx}(x_0) = y_{,xx}(x_L) = 0, \text{ and } q_{,x}(x_0) = q_{,x}(x_L) = 0 \tag{4}$$

Case 2: Fixed supported (wythe rotation is prevented)

The relative displacement between the wythes is prevented in this case, then

$$y_{,x}(x_0) = y_{,x}(x_L) = 0, \text{ and } q(x_0) = q(x_L) = 0 \tag{5}$$

Case 3: Fixed supported (wythe rotation is allowed)

The relative displacement between the wythes is prevented, but the wythe rotation is free. The moment in each wythe is therefore set to zero, and the total panel moment is calculated based on the relative displacement. Therefore, from Eq. (1), we get the following

$$y_{,xx}(x_0) = y_{,xx}(x_L) = 0, \text{ and } q_{,x}(x_0) = -\frac{2rM(x_0)}{\alpha^2 EI}, \text{ and } q_{,x}(x_L) = -\frac{2rM(x_L)}{\alpha^2 EI} \tag{6}$$

The connectors are embedded into the structural wythe, several end-restraint conditions for the connectors are possible depending upon the connector support provided by the wythes such as truss action; Fig. 4 shows three restraint conditions. The connecting layer stiffness  $K$  is computed for each of the foregoing three conditions as the force per unit area parallel to the wythes required to sustain a unit relative displacement between the wythes. For the connectors shown in Figs. 2 and 4 the tributary area is  $2rb/mp$ , where  $m$  = number of connector rows across the panel width,  $b$ ; and  $p$  = connector slope. In this case,  $A_c$  and  $E_c$  are connectors' area and elasticity modulus, respectively. The connectors are pinned at the center of each wythe.

For a unit relative shear deformation between the wythes, the elongation of the connector,  $e$ , is as follows

$$L = \frac{2r\sqrt{1+p^2}}{p}, \quad H = \sqrt{1+p^2}, \quad \cos \phi = \frac{1}{H} = \frac{1}{\sqrt{1+p^2}}$$

$$e = 1 \cdot \cos \phi = 1 \cdot \frac{1}{\sqrt{1+p^2}}, \quad e = \frac{1}{\sqrt{1+p^2}} \tag{7}$$

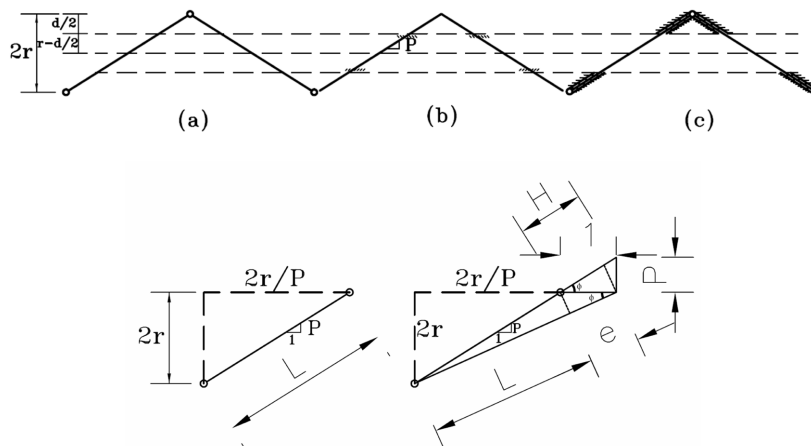


Fig. 4 Connector-embedment types: (a) pinned at wythe center, (b) fixed at wythe embedment, (c) laterally supported within wythe, (d) calculation the elongation

Multiplying by the connector stiffness gives the axial connector force,  $F$ , as follows.

$$F = \frac{E_c A_c}{L} \cdot e$$

$$F = \frac{E_c A_c p}{2r(1+p^2)} \quad (8)$$

The shear stiffness is the component of  $F$  parallel to the wythes, as follows

$$K = \frac{(F/e) \cdot m}{b \cdot (2r/p)}$$

$$K = \frac{A_c E_c p^2 m}{4r^2 b(1+p^2)^{3/2}} \quad (9)$$

The displacement caused by a uniform pure moment in section of the panel is  $M_T$ , to the sandwich panel. The solution to (1) and (3) for  $M = M_T$  and simple supports is the following

$$q(x) = -\frac{2M_T r \beta}{EI \alpha^2 \chi \cosh(\chi L/2\beta)} \sinh(\chi/\beta x); \quad y(x) = -\frac{M_T L^2}{8EI} \left\{ 2 \left( \frac{2\beta}{\chi L} \right)^2 \left[ 1 - \frac{\cosh(\chi/\beta x)}{\cosh(\chi L/2\beta)} \right] + 4 \left( \frac{x}{L} \right)^2 - 1 \right\}$$

Where  $L$  = overall length; and  $x$  = distance from the centerline of the panel.

The maximum deflection,  $\delta$ , occurs at the center of the panel ( $x = 0$ ), as follow

$$\delta = -\frac{M_T L^2}{8EI} \left[ 1 - \frac{2}{\psi^2} (1 - \operatorname{sech} \psi) \right] = \delta_0 \left[ 1 - \frac{2}{\psi^2} (1 - \operatorname{sech} \psi) \right] \quad (10)$$

Where

$$\delta_0 = -\frac{M_T L^2}{8EI}; \quad \text{and} \quad \psi = \frac{\chi L}{2\beta}$$

The displacement factor,  $\delta/\delta_0$ , for a simply supported panel assuming connector-embedment condition 1 and a connector slope of unity is computed as follows

$$\beta^2 = \frac{1}{1 + 12(r/d)^2}; \quad \chi^2 = \frac{2K}{Ed} = \frac{A_c m}{4\sqrt{2}r^2 b} \frac{E_c 1}{Ed} = \frac{1}{4\sqrt{2}} \frac{A_c m n}{r b} \frac{1}{rd} \quad (11)$$

Substituting the foregoing definition of  $\alpha$  and  $\beta$  into  $\psi$  gives the following

$$\psi^2 = \frac{1}{16\sqrt{2}} \left( \frac{L}{r} \right)^2 \left( \frac{A_c n m}{r b} \right) \frac{r}{b} [1 + 12(r/d)^2] \quad (12)$$

### 3. Design of specimens

#### 3.1 Assumption

The following assumptions are made for the design of the full-scale test panels:

1. Flexural reinforcement must yield prior to the failure of the shear connectors, compression, or shear failure of connectors.
2. Each panel is designed to resist against stripping and handling loads, that entire panel acts as a composite unit.

3. Steel connectors are sized to carry the shear force at the insulation and concrete interface.
4. Moment capacity is based solely on the welded wire fabric in tension zone; reinforcement in the compression zone is ignored.
5. Design compressive strength of the concrete is about 27 MPa at 28 days.

### 3.2 Connector design

Horizontal shear distribution over the length of the panel at ultimate strength is a function of the flexural shear  $V_u$ . The number of 3.5 mm steel bar connectors needed is calculated to provide an ultimate shear capacity to resist the applied loads assuming a full-composite panel.

### 3.3 Panel analysis

The present part provides calculation of the strength and stiffness of the tested panels. Composite behavior of the panels is evaluated by treating the panel like a plane truss. Each wythe is modeled as a beam element and the connectors are modeled using truss elements. The ultimate load is computed based on moment and shear capacity. An evaluation of cracking under service load is also given. Tests on cylinders poured and cured under the same conditions as the panels indicate that the actual strength of the concrete at 28 days is 28.7 MPa and the unit weight of the concrete is

Table 1 Design information parameters

$L$	2840 mm	$I_{wt}$	1872 mm <sup>4</sup>	$\epsilon_{cu}$	0.003
$b$	1040 mm	$A_{wb}$	4160 mm <sup>2</sup>	$\theta$	61
$h$	200 mm	$I_{wt}$	554.7 mm <sup>2</sup>	$\rho$	2260 kg/m <sup>3</sup>
$t_t$	60 mm	$y$	110 mm	$M_w$	2004 kN.mm
$t_p$	100 mm	$I_g$	58587 mm <sup>3</sup>	$M_u$	12351.5 kN.mm
$t_b$	40 mm	$Q$	3744 mm <sup>3</sup>	$M_p$	10347.5 kN.mm
$A_{wt}$	6240 mm <sup>2</sup>	$r$	150 mm	$f_y$	470 MPa

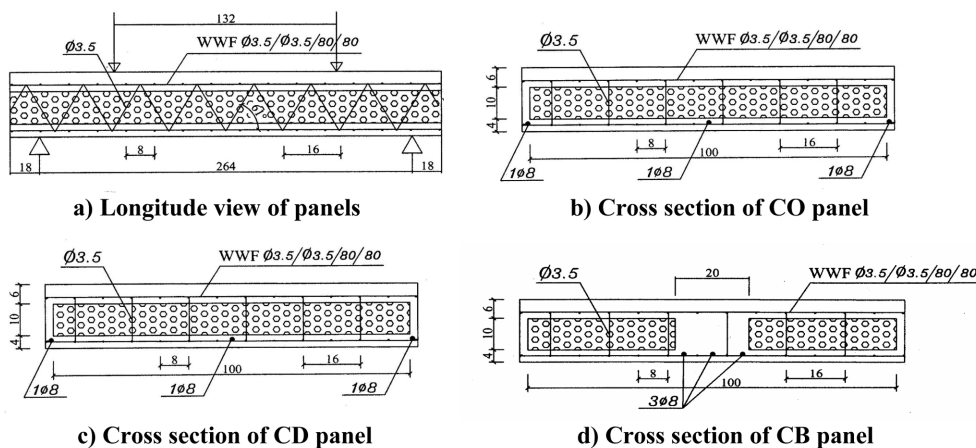


Fig. 5 cross section of specimen's type CO, CD and CB

2260 kg/m<sup>3</sup>. The concrete modulus of elasticity becomes  $E = 16$  GPa. The panel design parameters are given in Table 1. The parameters are corresponded in Fig. 5.

In which  $M_v$ ,  $M_u$  and  $M_p$  are internal moment due to panel self-weight, ultimate resistant moment and plastic moment of slabs sections, respectively. The stiffness and ultimate capacity of the truss connectors are based on linear analysis of the panel. Yielding of steel shear connectors in tension and buckling of those in compression tend to redistribute shear flow over the length of the panel as the most highly stressed connectors. The maximum load can be computed based on the entire shear capacity of the steel trusses over the length of the panel.

#### 4. Experimental studies

Three different types of specimens are cast. Each type includes three identical 3D floor panels. Fig. 5 indicate the longitudinal and transverse section of all types. Type CO is an ordinary plane 3D slab without additional reinforcement. Type CD is a reinforced type with  $3\phi 8@125$  mm, Fig. 5(c). The third one, CB type, is a longitudinally stiffened with a concentrated central beam, Fig. 5(d).

##### 4.1 Slab details

The specimens have 1000 mm width, 200 mm constant thickness including 60 mm of upper layer concrete with mix design of A, 40 mm thickness of shotcrete at the bottom surface and 100 mm of expanded polystyrene core. The welded wire fabric is considered of cold rolling of steel bar with final outside diameter 3.5 mm in accordance with ASTM A82 and automated welding process with accordance of ASTM A185. The yield and ultimate strength of drawn and annealed wires are 520 and 570 MPa, respectively. Elongation of mesh is 2.65% mm/mm. Fig. 6 shows the stress-strain curves for welded wire fabric and additional reinforced steel bars. The shotcrete used for all specimens, as designated by mix design B in Table 2, is used from Portland cement (II), river sand

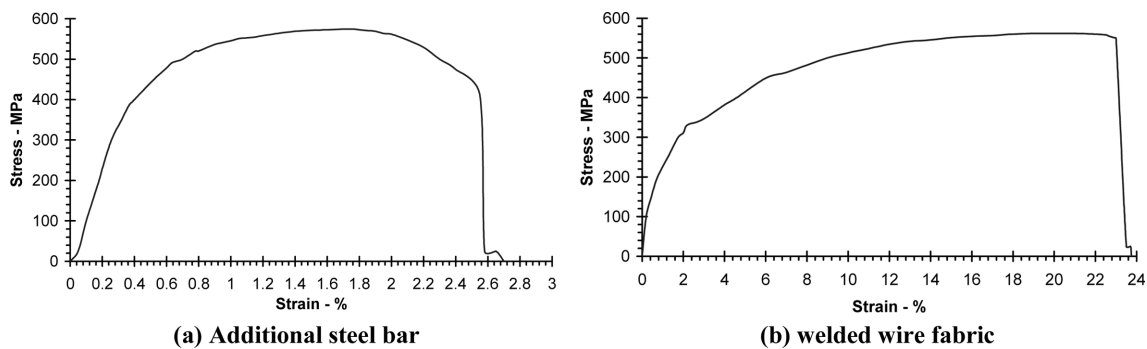


Fig. 6 Stress-strain reinforcement

Table 2 Concrete mix design

Units are in kg	Cement	Sand	Gravel	Water
A	350	700	1100	180
B	400	1700	-	200

with maximum 8 mm diameter, drinkable water. The W/C is about 0.45.

The maximum size of aggregate in upper wythe is about 15 mm and its fine modules is 2.5. Compression tests are carried out on (150\*150\*150 mm) standard cubes and provided cores from shotcrete. For each type of panel, there are six samples from longitudinal and transverse of welded wire for tensile test and weld strength provided.

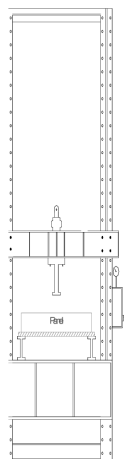
According to the result of test, compressive strength  $f_c$  is about 20 MPa for shotcrete and 27 MPa for concrete.

#### 4.2 Experimental test

Testing of panel specimens is performed in a horizontal position according to ASTM E72 as four point flexural loading test. Load is applied to the specimen by pumping oil into hydraulic jack. The displacement of the specimen is measured by dial gage. The applied load is monitored using a pressure gage mounted on the primary oil hose. Fig. 7 shows the schematic view of reaction frame for test set up and applying load. The test assembly is also pictured in Fig. 7(b).

The test procedure is as follows:

1. Lift the specimen using four lifting points and move it to the test site.
2. Place the specimen in the testing frame. Shim the specimen to provide snug contact with the reaction points.
3. Apply the static lateral load, gradually. Each loading step increment is 50 kg. For each increment, turn off the oil pressure and read the pressure and displacement.
4. Displacements are measured at both reactions for maintaining of horizontal position of specimen during the flexural test, and at 1/4, 1/2 and 3/4 of span, with the accuracy of 0.01 mm.
5. All measurements are continued until reaching to a maximum mid-span deflection for each type of specimen. Then, the load is slowly removed by reducing of oil pressure.
6. Remove the load and break the specimen to inspect the connectors inside the specimen.



(a) Side view



(b) test assembly

Fig. 7 Reaction frame used for applying flexural loading

### 4.3 Test results

Fig. 8 shows the load deflection curves for CO type panels. Also shown in Fig. 8 are the theoretical extremes of fully composite and non-composite as well as the theoretical prediction of load-deflection curve based on results of the linear analysis and non-linear numerical F.E.M approach. It is observed that up to 10.00 kN of applied load and its corresponding mid plane deflection of 2.5 mm, the load-deflection is proportional and no crack is detected. The bending stiffness is also constant as depicted in Fig. 9. Each of the panels shows a gradual loss of stiffness with increasing load. This loss of stiffness has three primary causes: 1) cracking of the concrete in the tension wythe, 2) cracking of the concrete in the connector embedment regions, and 3) deformation of the insulation. Cracking of the tension wythe results in a redistribution of the panel forces increasing the axial force in each wythe. Cracking of the concrete around the connector decreases the connector stiffness, redistributing of the wythe axial force into bending moment. Failure of the bond between insulation and the concrete wythes results in a loss of shear stiffness in the connecting layers. The insulation has only low shear stiffness, but the contact area is initially large enough to cause a significant contribution to the shear stiffness of the panel. The first factor

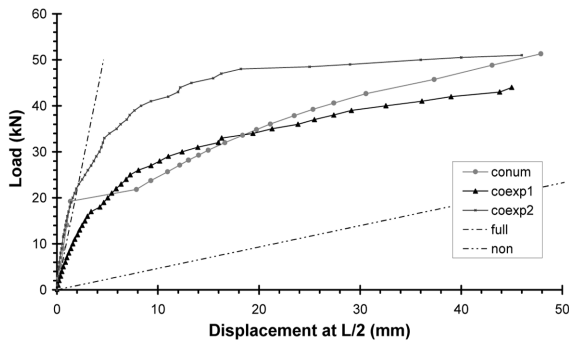


Fig. 8 Load deflection curve for CO panel

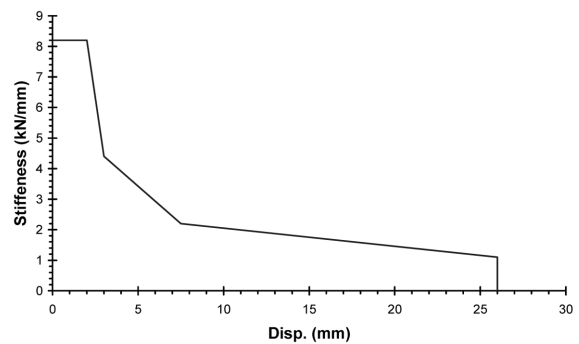
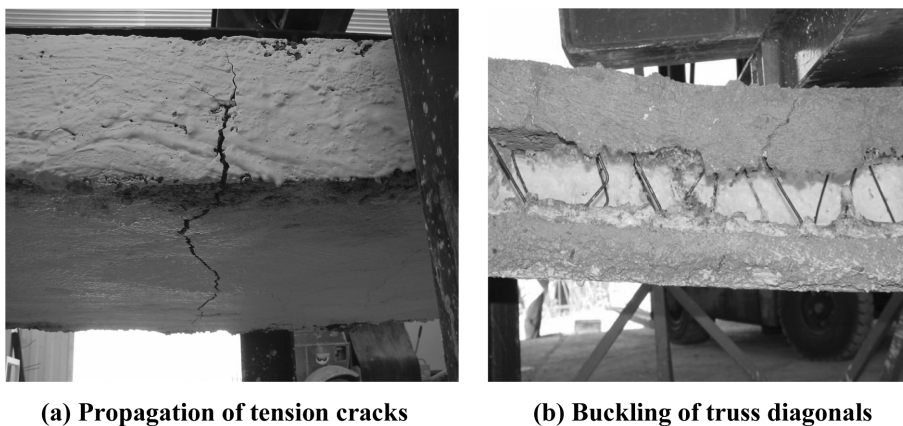


Fig. 9 Variation of bending stiffness during flexural loading for  $x = L/2$  in experiments for CO specimens



(a) Propagation of tension cracks

(b) Buckling of truss diagonals

Fig. 10 Failure mechanisms of 3D panels in flexural loading

occurs primarily near the center of the panel, while the second and third occur near the supports.

Fig. 10 shows the initiation of tension crack and its propagation to the upper layer. During this process, the failure of bottom welded wire mesh and detachment of lower wythe from insulation core are occurred. The truss connectors are approached to behave initially in an essentially semi-composite fashion, followed by a gradual decrease in stiffness as the load is increased. At higher level of loading, the loss of stiffness is more pronounced and it is due to the buckling of diagonals that are more in compression and are located in part of between reactions and applied loads. These results in only one-half of the truss diagonals effectively resisting the horizontal shear forces. This phenomena is revealed, after the test, by dissolving of insulation core and observing the buckled shear connectors. Also, due to the partial transmission of shear from top to bottom and non-composite performing of the section, it is measured that two wythes have a relative horizontal displacement about 22 mm.

The failure mechanism of experiments is adopted for modeling of slab in numerical analysis. It is also seen that the FEM analysis gives greater load-deflection path with similar trends. The reason for such behavior could not be clearly explained and could be due to micro-mechanical defects in shotcrete and test procedure. However, the ultimate strength in both numerical and experimental investigation is close to each other.

The same procedure for bending test is repeated in order to investigate the failure mechanism of type CD panel in which the bottom tension steel bars, as  $\phi 8@500\text{mm c/c}$ , are added to the welded wire fabric, WWF  $\phi 3.5/\phi 3.5/80/80$ , in order to increase ductility of panels. The obtained results show no remarkable differences between ultimate applied loads to compare to the previous type with no additional tension reinforcement. The maximum load is about 53.00 kN, 4% above the CO type. CD types of panels show more flexibility than CO type. Unlike CO panels suddenly failure, this type treated more flexible. It is concluded that in 3D sandwich panels subjected to flexural

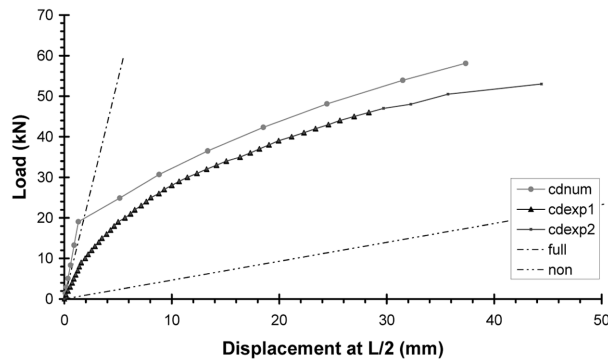


Fig. 11 Load deflection curve for CD panels

Table 3 Load-deflection results at linear and ultimate stages for CB type

Specimen No.	Linear portion		Ultimate	
	Load (kN)	Deflection (mm)	Load (kN)	Deflection (mm)
CB-1	20.50	2.49	83.00	39.5
CB-2	20.50	2.49	83.00	39.5
CB-3	30.00	1.99	92.50	26.53

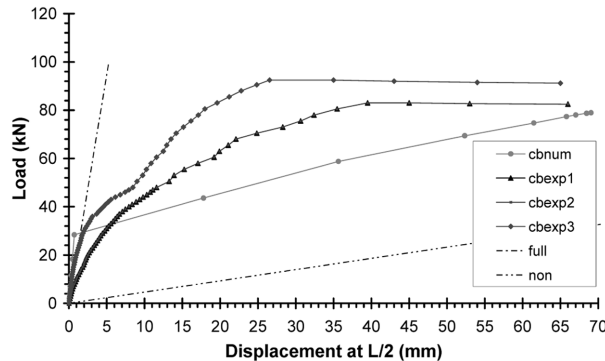


Fig. 12 Load-deflection curves for CB panels

loading, the governing failure mode is affected by failure of shear transferring from top layer to the bottom one. Buckling of shear connectors resting in elastic insulated media reflects this deficiency. Fig. 11 shows the load-deflection curve for CD type panel under vertical loading.

Type CB, is a stiffened 3D shotcreted slab stiffened with centrally horizontal beam and is subjected to transverse vertical loads. The experiments are revealed interesting results. Table 3 shows the loads and their corresponding deflection of CB type panels. Also, Fig. 12 represents the load-deflection path in laboratory tests. It is seen that up to 20.50 kN the total section behavior is linear and fully stiffness of the cross section is used for transferring applied loads. In other words, the section acts as fully composite. The deformation of mid-span for this region is 2.5 mm. Increasing loads results in a gradual loss of stiffness. The noise due to cracking of insulated polystyrene core is much limited compare to previous types, CO and CD. The lower welded wire is not broken. However, the steel bars,  $3\phi 8$  located at center are yielded.

Two obvious non-linear portions are observed in Fig. 12 before reaching to ultimate loads. In the first segment, the loss of stiffness is about 30% and related to the bottom concrete wythe cracks and failure of brittle core materials. The load reaches up to 48.00 kN. The corresponded vertical deflections are 8 mm and 12 mm for two specimens, respectively, Fig. 12. In the second non-linear segment, the bottom concentrated steel reinforcements are yielded. It should be considered that the extreme of full composite is different of CO and CD type. It is upper than another in CB type because of the more rigidity due to concrete beam. The concrete cracks propagate to the upper regions and more stiffness loss, about 65%, are detained. It is reported, after completing the test and dissolving of polystyrene, there is no buckling of shear connectors is observed. The ultimate load is upgraded to 1.8 times of plane slab without any additional reinforcement. The final mi-span deformation is increased to 65 mm. The presence of small concrete beam as stiffness of panel in 3D slab system makes more ductility and load carrying capacity and structural performance. In fact, panel CB type behaves like as I shape wide flange beam. The shear is transformed completely via concrete beam and diagonal shear connectors.

## 5. Numerical analysis and parametric studies

To extend the experimental investigation into wider application, numerical study is carried out using finite element analysis. Due to complexity of subject, the ANSYS software as a commercial

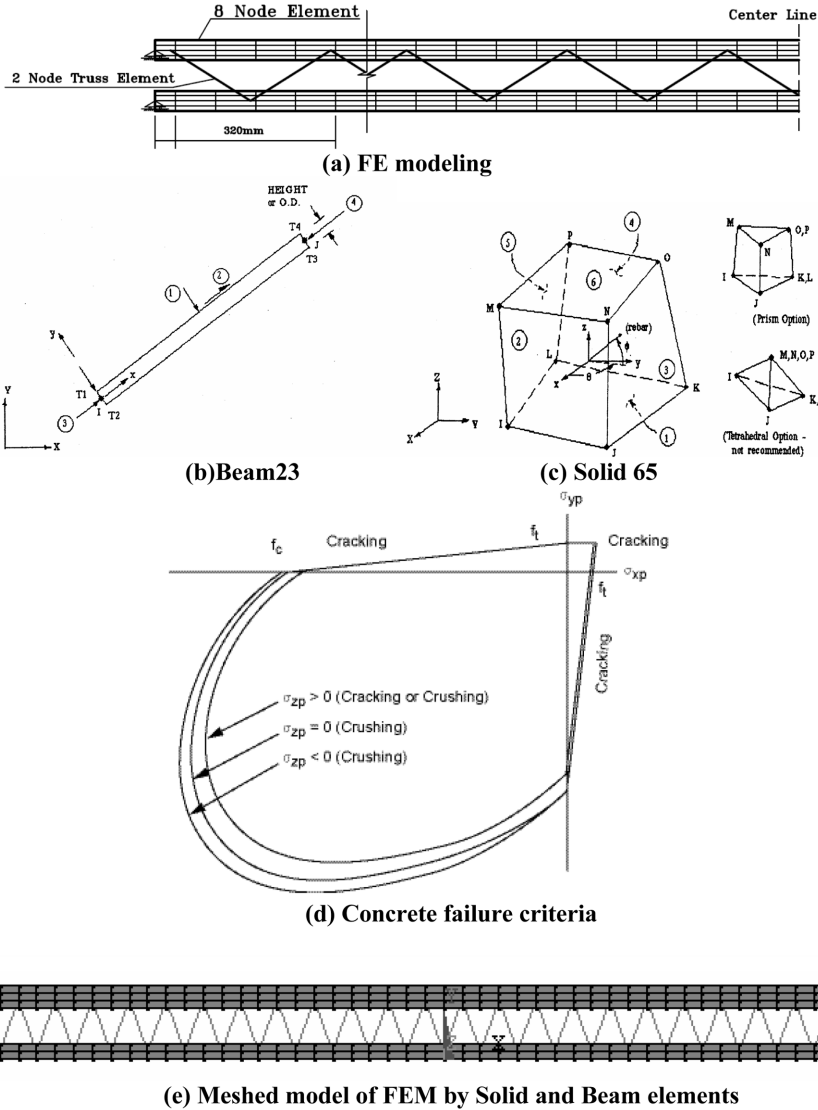


Fig. 13 Numerical shell models for analysis

F.E.M program with capability of geometrical and material non-linearity is used.

Sandwich panels are modeled as two concrete wythes which are connected by truss elements together. The appropriate elements from ANSYS library for modeling of concrete layers are selected as Solid65; an 8-node 3D brick element for modeling of concrete layer with potentially of crack development in three directions at Gauss integration points. Solid elements were modeled in various size and shape to find the best convergence of results. Beam23 is a two-dimensional beam element and used for modeling of bars and shear connectors, Fig. 13.

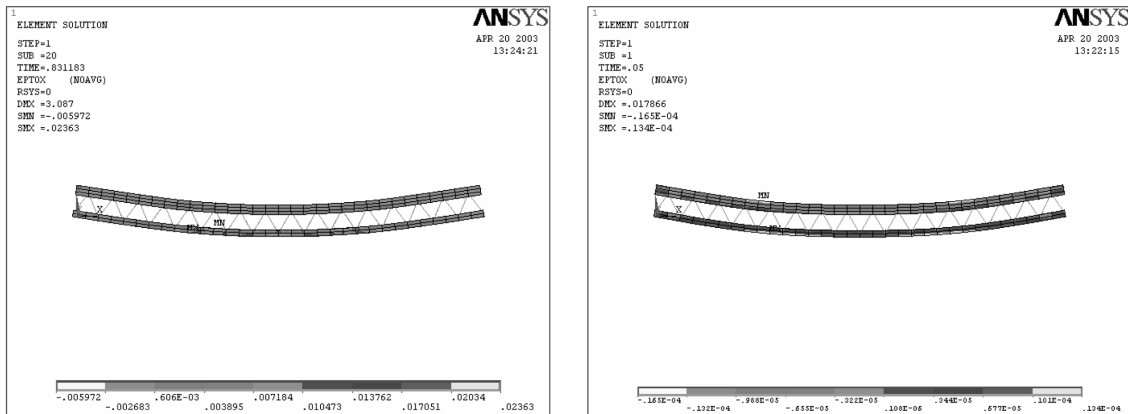
The concrete material model predicts the failure of brittle materials. The criterion for failure of concrete due to a multi-axial stress state can be expressed in the form (William and Warnke (1975))

$$\frac{F}{f_c} - S \geq 0 \quad (13)$$

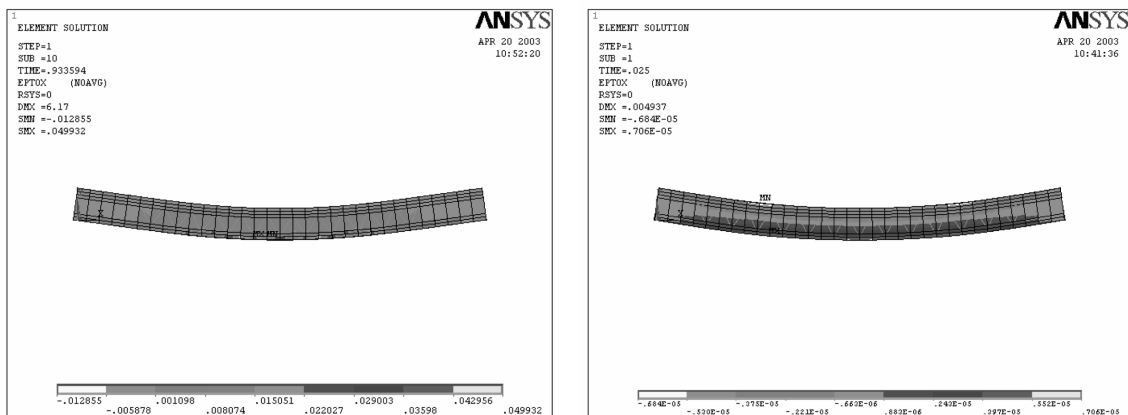
Where

- $F$  : a function (to be discussed) of the principal stress state ( $\sigma_{xp}$ ,  $\sigma_{yp}$ ,  $\sigma_{zp}$ )
- $S$  : failure surface (to be discussed) expressed in terms of principal stresses and five input parameters  $f_t$ ,  $f_c$ ,  $f_{cb}$ ,  $f_1$  and  $f_2$  defined as below
- $f_t$  : Ultimate uniaxial tensile strength
- $f_c$  : Ultimate uniaxial compressive strength
- $f_{cb}$  : Ultimate biaxial compressive strength
- $f_1$  : Ultimate compressive strength for a state of biaxial
- $f_2$  : Ultimate compressive strength for a state of uniaxial
- $f_c$  : uniaxial crushing strength
- $\sigma_{xp}$ ,  $\sigma_{yp}$ ,  $\sigma_{zp}$ : principal stresses in principal directions

Fig. 13(d) represents the 3-D failure surface for states of stress that are biaxial or nearly biaxial.



(a) CO panel



(b) CB panel

Fig. 14 Numerical analysis results

In addition, steel material is modeled by multi-linear kinematics properties as like as Fig. 6. Nonlinear behavior of steel rebars and meshes has completely isotropic materials.

The numerical models are provided to be compatible with geometrical, material load condition of prototype in experiments. To show satisfactory verification, the following comparison is presented for the mentioned three types panels. In all curves, the upper and lower bonds are sketched for full and non-integrated section, respectively.

Fig. 15 show the load-deflection curves representing flexural performance of 3D panels. Two different shear connectors diameter are considered as 3.5 and 4 mm to measure sensitivity on diagonal members. For all cases, it is observed that, in linear elastic level, the experiments and numerical results are almost corresponded to each other. In non-linear portion, it is seen considerable discrepancy of numerical analysis with respect to the experiments. The main reason for

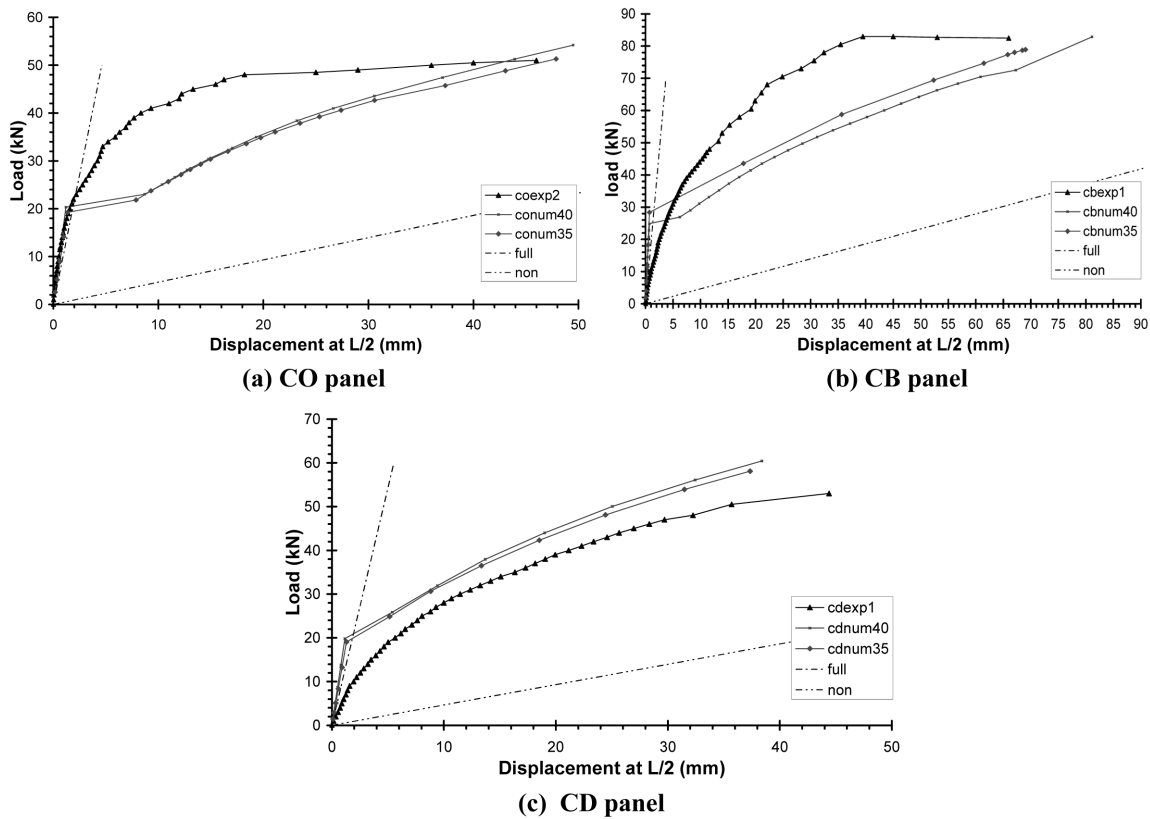


Fig. 15 Load-deflection diagrams in flexural 3D slabs

Table 4 Influence of reinforcement area on flexural performan

Specimen type	5T4	3T6	3T8
Steel rebar arrangement	5Ø4 mm c/c	3Ø6 mm c/c	3Ø8 mm c/c
Area (mm <sup>2</sup> )	62	85	115
Ultimate load (kN)	57.00	58.20	58.00
Deformation (mm)	48	49	37

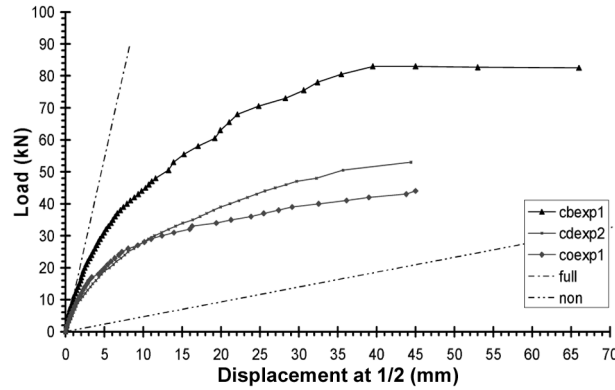


Fig. 16 Experimental study of panels

such difference is referred to sliding in smeared crack modeling in ANSYS. Although the ultimate load in both methods are close to each other. At the last stage of loading, the slope is almost flattening out, indicating failure mechanism. The major aspect, which could affect on failure is owing to the shear connector diagonal members, e.g. local instability. Comparing the load carrying capacity of three described panels in Figs. (a), (b) and (c) reveals inserting a longitudinal concentrated beam makes remarkable upgrading in ductility and load carrying capacity of 3D flexural panels, while, placing additional tension rebar only increase loading level.

The variation of additional tension rebars examined in CD panels in order to increase lateral load capacity and vertical ductility. Table 4 shows different reinforcement areas. These reinforcement sections are selected among some frequent analysis and it is seen that using more reinforcement does not necessarily give more strength and deformation. For every specified span length, the optimum reinforcement should be determined. Also, the failure of shear connectors affects remarkably on ultimate load of 3D sandwich slab and there is no big deal in gaining of additional load. The comparison results of flexural performance of mentioned three types of bearing slabs are presented in Fig. 16 based on experimental investigation. It is clearly observed the considerable superiority of 3D slab stiffened with a longitudinal central small beam. Since, the behavior is mostly brittle, adding a concentrated RC beam could enhance section shear capacity and prevent the premature fracture due to buckling of slender members.

## 6. Strain distributions

Study on strains across the section is performed from experimental measurement and numerical analysis in order to clarify the longitudinal displacement of cross section and calculation of bending strain profile. Fig. 17 shows the axial strains of CO and CB type panels at three stages of loading in middle of span from FEM results. At 19.25 kN of applied load, the strain distribution is linear and the section behaves in full composite fashion. The neutral surface is located between two concrete layers and the strain profiles for both upper and lower layers are parallel. At 25.70 kN, the neutral axis is shifted towards compressive upper layer and strain is not linear. Increasing the applied load to 42.50 kN, the neutral line is moved to near upper edge of panel, about 17.5 mm below, and the strain at the lower edge of upper wythe is reached to 0.0023 close to  $\epsilon_{cu}$ . The semi-composite and

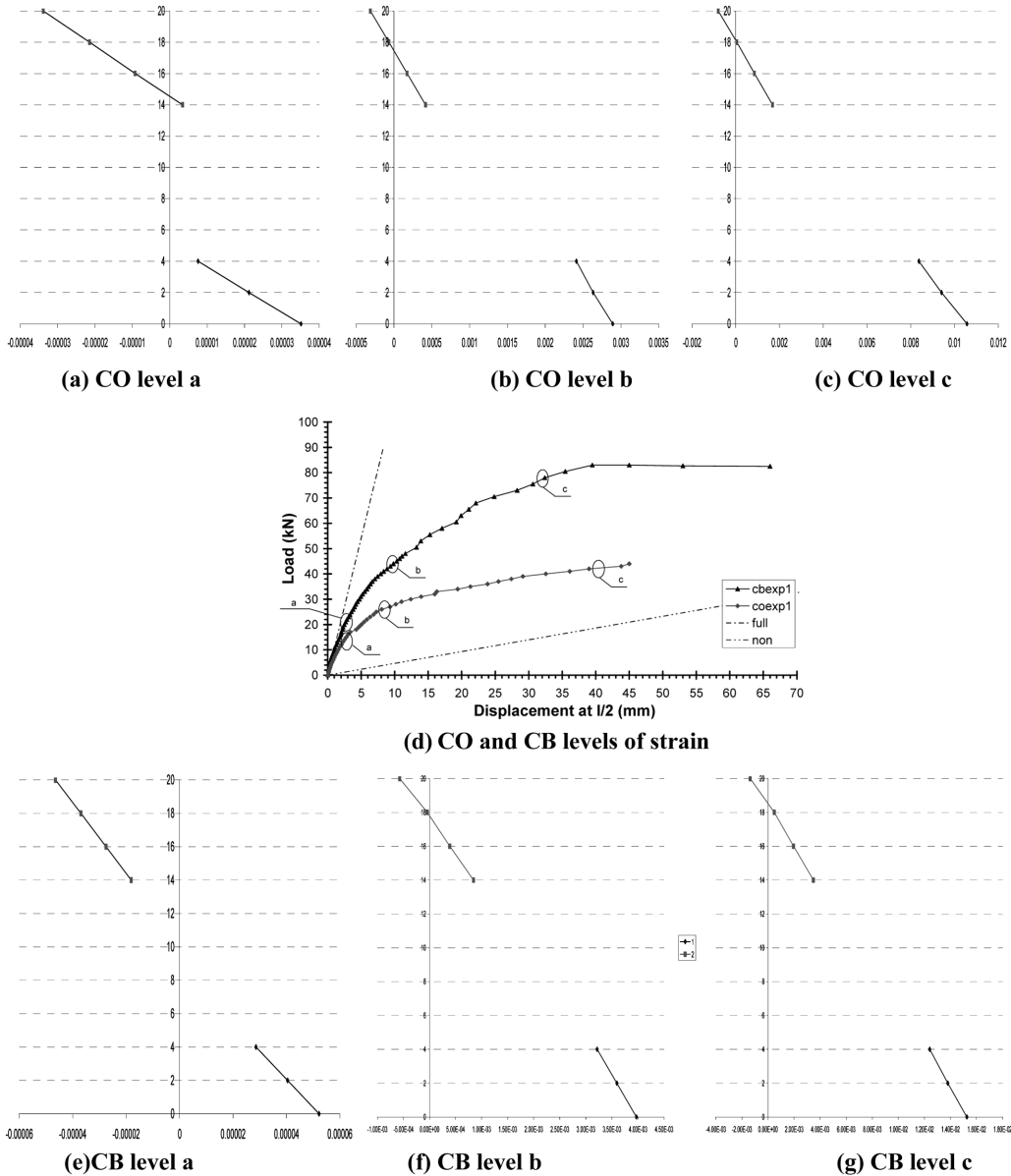


Fig. 17 The FEM bending strain distribution of cross section in CO type panel for three stages of loading

non-composite in Figs. 17(b) and 17(c) represent the bending performance of the section and it could be used for design calculation of moment of inertia.

In CB type, Fig. 17(e) to 17(g), at load stage of 18.31 kN the section acts as fully composite. The strain distribution for 43.75 kN of applied load is quasi-linear, but the section is in semi-composite condition. The neutral axis is placed in upper concrete layer. At 76.00 kN of loading level, the total bottom layer is in tension; however, the neutral surface is close to upper edge of concrete.

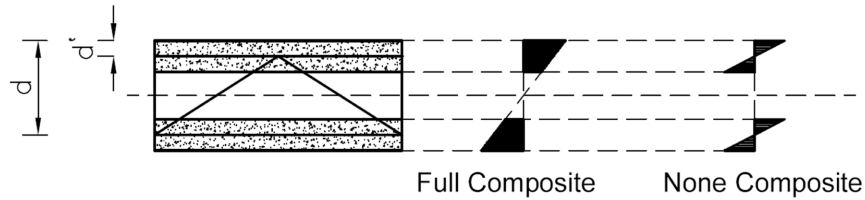


Fig. 18 Section of specimen in two types, full composite and none composite

### 7. Theoretical flexural capacity

In design code, the flexural behavior of beams is calculated based on full bonding of the cross section, Fig. 18. In this direction, the ultimate bending moment of a 3D panel is obtained based on equilibrium equation, (ACI 98-506)

$$A_{s1}f_{s1} + A_{s2}f_{s2} - A_{s1}f'_c = 0.85f'_c ba \tag{14}$$

In which:

- $A_{s1}$  : area of upper steel
- $f_{s1}$  : upper steel force
- $A_{s2}$  : area of lower steel
- $f_{s2}$  : lower steel force
- $f'_c$  : concrete compressive strength
- $B$  : width of specimen
- $a$  : height of Whitney stress rectangular

It is assumed that all reinforcement including welded wire mesh and tension rebars are yield, so

$$M_n = 0.85f'_c ba \left( d - \frac{a}{2} \right) - A_{s1}f'_{s1} (d - d') \tag{15}$$

Where:

$M_n$ : flexural resistant moment

Therefore, the ultimate bending moments due to the lateral load for two types of slabs are tabulated in Table 5 as follows

The difference between experimental and theoretical results is referred to the approximate assumption of Whitney compressive block in top layer concrete portion.

Table 5 Comparing the analytical and experimental moments

Measurement	Experiment (kN·m)	Theory (kN·m)
CO	1580	1235
CD	2850	2097

## 8. Conclusions

The current study focuses on upgrading ductility and load carrying capacity of 3D slabs in two different ways; 1) using additional tension reinforcement, CD type panels, 2) Inserting a longitudinal concentrated beam, CB type panels, in order to improve their failure mechanism.

Based on experimental and numerical results, the following conclusions are raised:

- The failure mechanism of normal panel, CO type, is governed by shear mechanism of diagonal members and the collapse at ultimate load is mostly in brittle mode.
- Enhancing the 3D slab section with additional tension reinforcement could not remarkable increase in load carrying capacity as well as flexural ductility.
- Inserting a longitudinal concentrated beam at the centre improve considerable flexural and shear strength of the section and increase load carrying capacity in bending 3D elements.
- For specific given dimension, CB type panel carries vertical load about 100% more than normal panel and extend vertical deformation about 50%.
- The strain distribution shows more section bonding when it is stiffened with concentrated small beam.

The results of current studies could be useful in design consideration of such composite sandwich panels.

## Acknowledgments

The authors appreciate the financial support for current work from Prefabricated Sandwich Panels, SAP Company in Tehran.

## References

- ACI Committee 318 (1995), "Building code requirements for structural concrete and commentary".
- Bush, Thomas D. and Wu, Z. (1998), "Flexural analysis of prestressed concrete sandwich panels with truss connectors", *PCI J.*, **43**(5), 76-86.
- Benayoune, A., Aziz, A., Samad, A., Trikha, D.N., Ali, A. Abdullah Abang and Ashraborty, A.A. (2006), "Structural behaviour of eccentrically loaded precast sandwich panels", *Construction and Building Materials*, Elsevier.
- Building Code Requirements for Reinforced Concrete (ACI 318-95) (1995), American Concrete Institute, Detroit.
- Bush, T.D. and Stine, G.L. (1994), "Flexural behavior of composite precast concrete sandwich panels with continuous truss connectors", *PCI J.*, **39**(2), 112-121.
- Einea, A., Tadros, M.K., Salmon, D.C. and Culp, T.D. (1994), "A new structurally and thermally efficient sandwich panel system", *PCI J.*, **39**(4), 90-101.
- Einea, A., Salmon, D.C., Tadros, M.K. and Culp, T. (1995), "Partially composite sandwich panel deflection", *J. Struct. Eng.*, ASCE, **12**(940), 778-783.
- Ghali, A. and Neville, A.M. (1989), "Structural analysis: A unified classical and matrix approach", Third Edition, Chapman and Hall, New York, N.Y.
- Holmberg, A. and Palm, E. (1986), "Behavior of load bearing sandwich-type structures", Handout No. 49, State Institute for Construction Research, Lund, Sweden.
- Kabir, M.Z. (2005), "Structural performance of 3D sandwich panels under shear and flexural loading", *Scientia*

- Iranica Journal*, Article in press.
- Kabir, M.Z. and Hasheminasab, M. (2002), "Mechanical properties of 3D wall panels under shear and flexural Loading", CSCE Conference, June 5-8, Montreal Canada.
- Kabir, M.Z. and Rahbar, M.R. (2005), "Experimental relation between non-destructive test and standard cylinder in shotcrete used in bearing 3D wall panels", *Third Int. Conf. on Construction Materials*, Vancouver, Canada, August 22-24.
- Nijhawan, J.C. (1998), "Insulated wall panels Interface shear transfer", *PCI J.*, 98-101.
- PCI Committee on Precast Concrete Sandwich Wall Panels, "State of the art of precast/prestresses sandwich wall panels", *PCI J.*, 42(2), 92-133, 1997.
- Salmon, D.C., Eiena, A., Tadros, M.K. and Culp, T.D. (1997), "Full scale testing of precast concrete sandwich panels", *ACI J.*, 94, 354-362.
- Willam, K.J. and Warnke, E.D. (1975), "Constitutive model for the triaxial behavior of concrete", *Proc., Int. Association for Bridge and Structural Engineering*, 19, ISMES, Bergamo, Italy, p. 174.